Magnetophotoluminescence of $GaN/Al_xGa_{1-x}N$ quantum wells: Valence band reordering and excitonic binding energies

P. A. Shields and R. J. Nicholas
Department of Physics, Oxford University, Clarendon Laboratory, Parks Road, Oxford, OX1 3PU, United Kingdom

N. Grandjean and J. Massies
CNRS, Centre de Recherche sur l'Hétéro-Epitaxie et ses Applications, Valbonne, F-06560, France
(Received 8 January 2001; published 6 June 2001)

A reordered valence band in $GaN/Al_xGa_{1-x}N$ quantum wells with respect to GaN epilayers has been found as a result of the observation of an enhanced g factor ($g^* \sim 3$) in magnetoluminescence spectra in fields up to 55 T. This has been caused by a reversal of the states in the strained $Al_xGa_{1-x}N$ barriers thus giving different barrier heights for the different quantum well hole states. From k-p calculations in the quasicubic approximation, a change in the valence band ordering will account for the observed values for the g factors. We have also observed the well-width dependence of the in-plane extent of the excitonic wave function from which we infer an increase in the exciton binding energy with the reduction of the well width in general agreement with theoretical calculations of Bigenwald *et al.* [Phys. Status Solidi B **216**, 371 (1999)] that use a variational approach in the envelope function formalism that includes the effect of the electric field in the wells.

DOI: 10.1103/PhysRevB.63.245319 PACS number(s): 78.67.De, 71.35.Ji, 78.55.Cr

I. INTRODUCTION

The recent understanding of the influence of macroscopic polarization in nitride materials has inspired a closer look at the properties of $Al_xGa_{1-x}N$-based quantum wells where these effects are stronger than found with the more commercially attractive $In_xGa_{1-x}N$ system.

The typical optical characterization of a $GaN/Al_xGa_{1-x}N$ quantum well sample finds a single peak in luminescence at energies that are strongly dependent on the width of the wells and the aluminum content of the barriers. The energies of these peaks have been quantitatively understood in terms of the quantum-confined stark effect from which the electric field caused by the polarization can be deduced. It has been found that the field has a strong linear dependence on the aluminum concentration reaching almost 1.5 MV/cm for an Al composition of 27%.[1,2]

The optical quality, as determined from the emission efficiency, is better in the $In_xGa_{1-x}N/GaN$ system compared to the $GaN/Al_xGa_{1-x}N$ structures, whereas for the emission linewidth the opposite is true. The latter is likely to be related to the position of the ternary alloy in the structure, it being in the active region in $In_xGa_{1-x}N$ structures where an inhomogeneous composition would have a greater effect. Typically the best linewidths in $In_xGa_{1-x}N/GaN$ structures are about 40 meV,[3] which can be compared with about 20 meV for $GaN/Al_xGa_{1-x}N$ wells.[1] The development of these high-quality $Al_xGa_{1-x}N/GaN$ quantum wells (QW's) has now allowed measurements to be made of the magneto-optical properties in nitride-based quantum wells.

Due to the linewidths already mentioned, the large effective masses and the large exciton binding energies in these materials, it is necessary to use very high magnetic fields to see any effects. This leads us to use pulsed-field magnets that can currently give fields of up to 55 T.

II. EXPERIMENT

We have performed magneto-optical experiments in both steady and pulsed magnetic fields on single quantum well samples with different widths of 4, 8, 12, and 16 monolayers (ML). One monolayer corresponds to 2.59 Å therefore giving about 10, 20, 30 and 40 Å, respectively. The three samples described in this paper are described in Table I. The structures were grown by molecular beam epitaxy on GaN templates on sapphire substrates with 200 nm of $Al_xGa_{1-x}N$ grown as a buffer layer before the quantum wells. For samples N298 and N307, the technique of epitaxial lateral overgrowth (ELOG) was used to improve the template quality.[4] The sample widths and the aluminum composition were determined through reflection high-energy electron diffraction spectra observed during the growth.[5] The magnetic field was parallel to the hexagonal c axis of the crystal, and perpendicular to the plane of the quantum wells. Excitation and detection were carried out at normal incidence.

The results that will be discussed are low- and high-excitation photoluminescence (PL) with fields up to 55 T at 4.2 K where the effects of the field can be seen through a shift of the luminescence peaks. For the high excitation density PL the source was a pulsed (5 ns) frequency-quadrupled Nd:YAG (yttrium aluminum garnet) laser at 266 nm,

TABLE I. Details of the samples grown by molecular beam epitaxy (MBE).

Sample	Description
N257	4 SQW's of 4, 8, 12, 16 ML separated by 100 Å of $Al_xGa_{1-x}N$ at 13%. MBE template.
N307	SQW of 8 ML wide with $Al_xGa_{1-x}N$ barriers with 8% Al. ELOG template.
N298	4 SQW's of 4, 8, 12, 16 ML separated by 100 Å of $Al_xGa_{1-x}N$ at 8%. ELOG template.

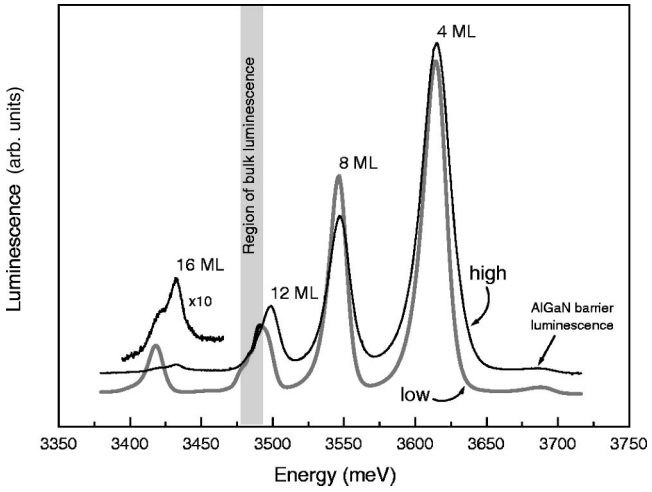

FIG. 1. High- and low-excitation photoluminescence of sample N257 from four separate quantum wells, of widths 4, 8, 12, 16 monolayers (10, 20, 30, 40 Å) scaled for a comparison of the peak positions.

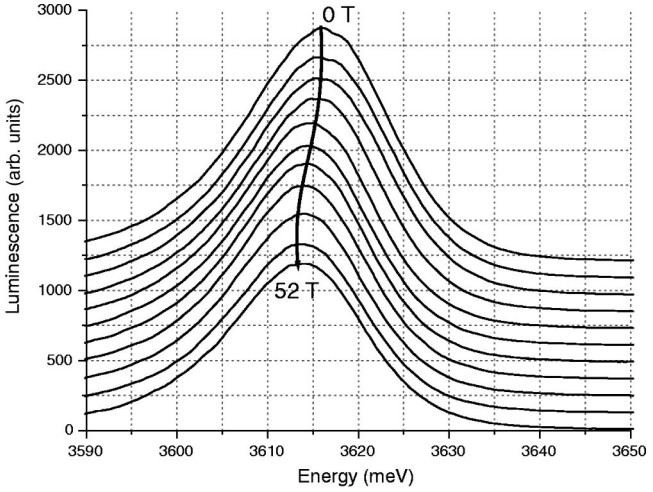

FIG. 2. Magnetic field dependence of the low-excitation photoluminescence for the 4 monolayer quantum well in sample N257. The spectra are offset for clarity.

whereas for the low-excitation density it was the 244-nm line from a cw frequency-doubled argon laser. For the latter in the pulsed fields, a masked chopper wheel was used to produce a train of short laser pulses, ~0.3 ms duration, at ~100 ms intervals. A pulse from this train triggered the magnet system so that the next laser pulse coincided with the maximum of the pulsed field, where there is little change in the field ($\leqslant 1\%$) over a 0.3-ms time scale. A charge-coupled device cooled to $-70\,^{\circ}\mathrm{C}$ attached to a quarter meter spectrometer was used to detect the PL.

III. RESULTS

Figure 1 shows the low- and high-excitation PL for sample N257. Several PL peaks can be seen that can be attributed to the different wells. Between the low and high excitation, we have observed a shift in the PL that is strongly dependent on the width of the wells, ranging from 1 meV for the narrowest up to 20 meV for the widest. This is in agreement with the idea that in-built electric fields play an important role in this sample via the quantum-confined Stark effect[6] and that they have been screened by the excited carrier population. Previous measurements have calculated the field to be ~550 kV/cm.[1] The most obvious consequence of this is seen through the observation of PL from the widest well at 3.42 eV, which is below the band gap energy of bulk GaN at 3.49 eV. Unfortunately, for this sample, the bulk feature coincides with the PL from the 12 ML QW, so that luminescence from the bulk template superimposes a structure onto this peak.

The low-intensity excitation is of the order 0.25 $\mathrm{W\,cm^{-2}}$ and can be considered to be in the regime where self-screening of the electric field is negligible. The exact excitation intensity of the pulsed laser is difficult to determine precisely, but can be estimated to be greater by about five orders of magnitude. The magnetic field results discussed below were therefore taken using the low-intensity quasi-CW excitation.

The effect of the magnetic field on the 4ML QW in sample N257 can be seen in Fig. 2, and shows a shift of the luminescence to lower energy. The form of this shift is dependent on the width of the wells, and is shown in Fig. 3. In order to determine the peak positions a center-of-mass method was used in preference to a peak-fitting routine.[7] This decision resulted from the difficulty of deciding the correct form of the peak as it is slightly asymmetric and thus causes problems for a Gaussian fit. The center of mass is also known as the first moment, and is given by

$$M_1 = \frac{\int I(E)E\,dE}{\int I(E)\,dE}. \tag{1}$$

For the spectra with several peaks, the minima between them at zero field were chosen as the boundary conditions for this routine. Since it is the shift with magnetic field that is required rather than absolute positions of the peaks, this is valid because the intensity at these points does not change significantly with field ($\lesssim 1\%$ of peak intensity).

For the widest wells there is a diamagnetic blueshift of the transition energy, but as the well width decreases we observe a transition to a redshift, which for the 4-ML well is approximately 2 meV at 50 T. Eventually at the highest field the redshift stops and appears to be overtaken by a smaller diamagnetic term.

For the widest well, two components are observed that have different dependencies on magnetic field. The observation of two peaks has previously been suggested to be due to fluctuations in the well width, corresponding to 16 and 17 ML. We see an enhancement of the 16-ML peak with field so that it dominates the spectra at high field, which is consistent with this proposal and the suppression of the in-plane transport. The excitons are then less able to find the potential minima caused by the fluctuations before recombining.

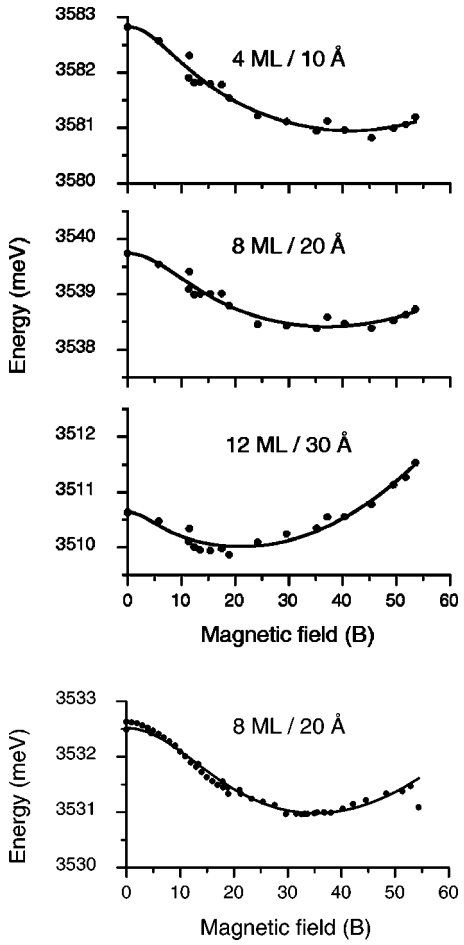

FIG. 3. Magnetic field dependence of the low-excitation photoluminescence for the different quantum wells for sample N298 (top) and N307 (bottom), along with the fits to the data as described in the text.

The shifts for all the wells can be described by the expression, $E(B)=E_0\pm\frac{1}{2}g^*\mu_B B+\gamma_2 B^2$ so that the overall dependence for each Zeeman-split component is determined by the relative magnitudes of the linear Zeeman and quadratic diamagnetic terms. The linear Zeeman shift causes the transition to split into two, of which we see predominantly the lowest energy component. The S shape observed especially for the narrower wells at the lower fields can be explained as resulting from a significant thermal population in the upper component whilst the Zeeman splitting is still small. This effect is particularly noticeable when the width of the luminescence is large compared with the shift in magnetic field and kT, as is the case in these samples.

The magnetic field dependence of the center of mass can then be expressed in terms of the populations in each component, $n\uparrow$ and $n\downarrow$,

$$E=E_0+\tfrac{1}{2}g^*\mu_B B\left(\frac{n\uparrow-n\downarrow}{n\uparrow+n\downarrow}\right)+\gamma_2 B^2, \qquad (2)$$

with the ratio $n\uparrow/n\downarrow$ given by a Boltzmann distribution. Table II shows the values deduced from the experiments for the characteristic temperatures, g factors and diamagnetic shift coefficient. These last two parameters will be individually discussed in the following sections. The temperatures deduced simply reflect a heating of the carriers by the high-excitation intensities onto the sample. These were necessarily rather high in order to detect sufficient signal in the short time duration of a single pulse ($\sim$0.3 ms).

TABLE II. The magnetic field fitting parameters for the different GaN/$Al_xGa_{1-x}N$ samples along with a bulk reference.

Sample N257	T (K)	g^*	$\gamma_2(\mu$ eV/$T^2)$
4-ML QW	15(1)	3.1 (1)	0.99 (7)
8-ML QW	13(1)	2.9 (2)	1.3 (1)
12-ML QW	13(1)	3.3 (3)	2.1 (2)
16-ML QW	5(5)	1.8 (4)	3.0 (3)
N298			
4-ML QW	9(3)	3.1 (2)	1.1 (1)
8-ML QW	8(3)	2.5 (2)	1.0 (1)
12-ML QW	5(5)	2.0 (2)	1.4 (1)
N307			
8-ML QW	17(3)	3.4 (2)	1.5 (1)
G889			
Bulk		0	2.04 (3)

IV. DISCUSSION

A. Zeeman splitting

The g factors for the different samples are compared in Fig. 4, and show a general trend towards $g^*\sim 3$ for the narrower wells, with it reducing to $g^*\sim 2$ for the wider wells. This is particularly noticeable in sample N298.

The observation of a Zeeman splitting through a clear redshift is surprising, since in the magneto-reflectivity of GaN epilayers, no such splitting is seen. From the results in bulk GaN the lowest transition, associated with the A va-

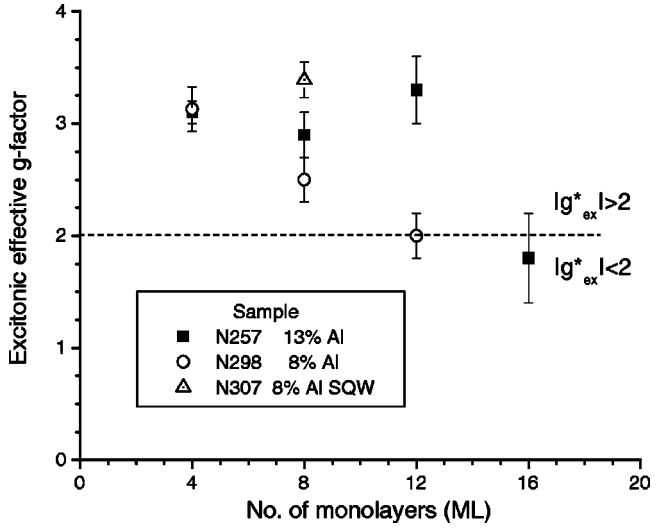

FIG. 4. The experimentally determined well-width dependence of the g factors.

lence band, does not split for the same orientation as the experiments described here.[8,9] This is due to a cancellation of the electron and hole g factors when the magnetic field is parallel to the c axis. Even for the B valence band there is a similar compensation leading to an excitonic g factor, $g^* = 1.24$. So as both theoretical and experimental work on $Al_xGa_{1-x}N$ heterojunctions[10] suggest that the electron effective g factor should not change from a value of ~ 2 as a result of confinement, we conclude that instead the hole g factor must have drastically changed in the narrower quantum wells due possibly to a significant change in the valence band structure.

The reduced symmetry of the wurtzite with respect to the cubic structure is represented in the Hamiltonian through the crystal field. If spin-orbit effects are neglected, the crystal field reduces the degeneracy of the valence bands with different z components of orbital angular momentum. With spin-orbit terms included there are then the three usual bands; A, B, and C with symmetries Γ_9, Γ_7, and Γ_7, respectively, that have the following separations:

$$E_A - E_{B,C} = \frac{1}{2}\left\{ (\Delta_{cr} + \Delta_{so}) \mp \left[(\Delta_{cr} + \Delta_{so})^2 - \frac{8}{3}\Delta_{cr}\Delta_{so} \right]^{1/2} \right\}, \tag{3}$$

where Δ_{cr} and Δ_{so} are the crystal field and spin-orbit energy terms, respectively.[11]

This is for the case of a bulk semiconductor. With the effects of a two-dimensional quantum confinement, the energies are usually understood in terms of the envelope function approximation that are then dependent on: the effective masses in the well and barrier, the valence band potential, and the width of the well. This causes the energies of the bands to become unrelated to the bulk energy terms in Eq. (3). Instead effective spin-orbit and crystal field terms can be used to account for the splittings of the A, B, and C valence bands, where the nomenclature is now strictly in terms of the band symmetries and not the ordering.

For the $GaN/Al_xGa_{1-x}N$ system, it is known that in bulk AlN the crystal field splitting has the opposite sign to that of GaN thus inverting the order of the states. This would lead to a reversal of the states at some critical value of x in $Al_xGa_{1-x}N$,[12] though this value is not experimentally known. The more important consequence for this work is that this will cause different valence band offsets for the different bands and Fig. 5 shows how this effect can lead to a reversal of the quantum well states, even when the same masses in the z direction, $m_\parallel$, are used. (In fact $m_\parallel$ is identical for the A and B valence bands.) This calculation was carried out for a symmetrical quantum well, which is known to be invalid for these samples. However the effect of a strong electric field will be to bring the confinement energy closer to the barrier offsets thus making them more important and enhancing the reversal effect.

A reversal of states has a profound effect on the spin ordering of the valence band that can be clearly seen through the results of calculations in Fig. 6. These were calculated using the Luttinger approach[13] within the quasicubic model at a magnetic field of 60 T, using the band parameters de-

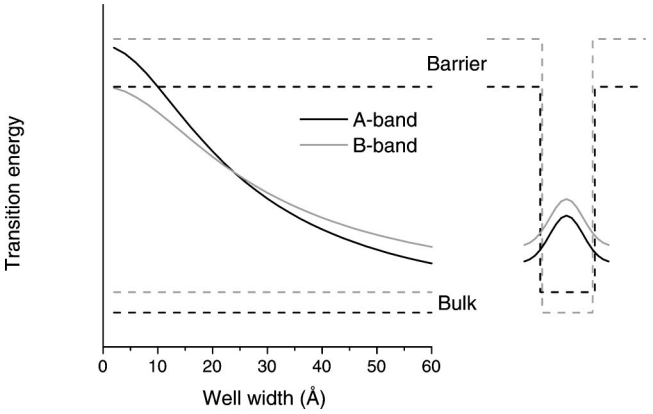

FIG. 5. A schematic diagram based on a finite quantum well model showing how the quantum well energies can cross at a particular well width for two bands with different offsets.

duced by Stepniewski *et al.*[9] With this model, the wurtzite Hamiltonian can be approximated as a cubic Hamiltonian that is uniaxially strained along the [111] direction. The *crystal field* from the wurtzite vocabulary can then be translated into a heavy-hole–light-hole splitting (HH-LH) in cubic language. Therefore with zero strain, corresponding to zero HH-LH splitting or zero crystal field, we find the usual zinc-blende band and spin ordering. The bulk wurtzite case is also indicated, corresponding to a finite strain or crystal field, and this correctly reproduces the spin ordering in GaN,[9] whereas AlN would correspond to the far right of the graph with a large positive HH-LH splitting. The crossing, or more correctly anticrossing, of the Γ_7 states causes a reversal of the spin ordering thus changing the sign of the g factor for the lowest[14] Γ_7 hole band. This process also lowers its energy below the Γ_9 A valence band so that transitions involving this band are favored in luminescence. Excitonic g factors less than 2 occur for the lowest bands to the left of the anticrossing in Fig. 6 as indicated, whereas they are greater than 2 to the right.

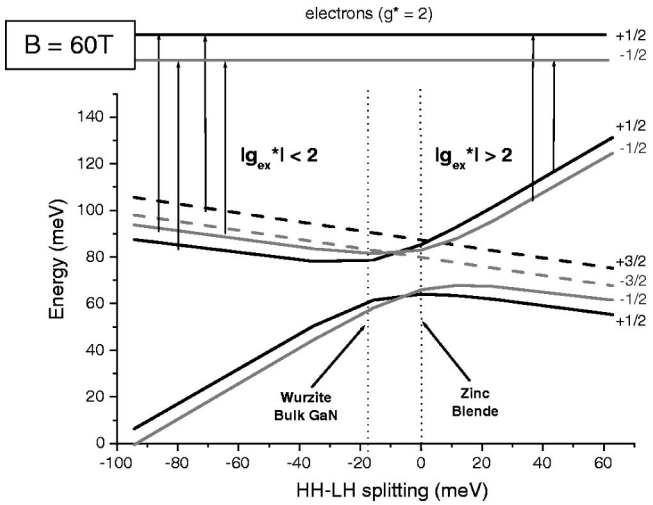

FIG. 6. The effect of the crystal field on the spin ordering of the valence band and the resulting g factors. Γ_7 states are indicated as solid lines, and Γ_9 states are dashed. The vertical arrows show the allowed optical transitions.

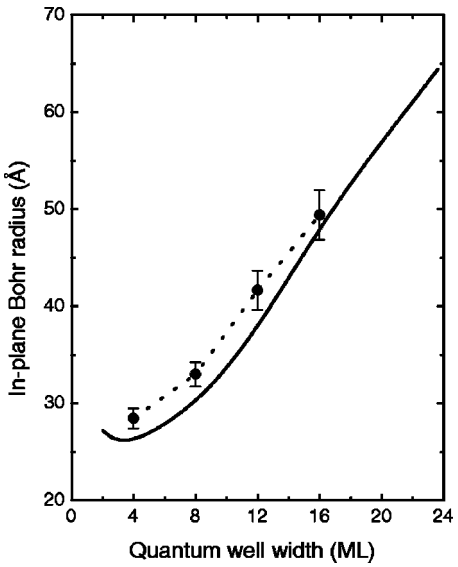

FIG. 7. Comparison between the experimental (points) and theoretical values (solid line) for the in-plane extent of the excitonic wave function for different well widths. The theoretical values are determined from considering a two-parameter variational trial function for a series of GaN/$Al_xGa_{1-x}N$ QW's with Al barrier composition $x=0.27$. The experimental values are from sample N257 and are deduced from the diamagnetic shift of the luminescence.

For a GaN/$Al_xGa_{1-x}N$ quantum well structure the precise band ordering of the confined states is hard to predict since it is critically dependent on both the well and barrier properties due to the electric field. As an extra tool, x-ray measurements can be used to examine the crystal properties and give information on the strain that is present. In these samples, it has been shown that the $Al_xGa_{1-x}N$ barriers have the same in-plane lattice constant as the GaN template, it being larger than if they were unstrained, resulting in them having a tensile biaxial strain.[1] Therefore the well material is unstrained and has a normal wurtzite GaN valence band structure, whilst the barrier has the opposite ordering due to the AlN contribution in the alloy and the strain present.

The latter can be estimated from using a linear relationship for the lattice constant, giving an in-plane strain, $\varepsilon_{xx}=\varepsilon_{yy}=0.31\%$ for an aluminum content of 13%. This contributes to the crystal field splitting through $\Delta_{cr}+\frac{3}{2}D_3\varepsilon_{zz}$ with $\varepsilon_{zz}=-2C_{13}/C_{33}\varepsilon_{xx}\approx-0.51\varepsilon_{xx}$, and $D_3\sim 6$ eV to give $\frac{3}{2}D_3\varepsilon_{zz}=14$ meV.[12] As experimental values of Δ_{cr} for GaN are very close to this value (11–15 meV),[15] once the contribution of the AlN is also included, the barriers are very much in the regime for a reversal of states to occur. Figure 7 of Kim *et al.*[12] shows a calculation for a similar tensile biaxial strain in GaN that clearly shows a reversal of the states with the anticrossing also giving the lowest valence band a heavier mass than would be otherwise expected.

Therefore our results suggest that the ordering of the valence band has changed for narrow quantum wells, perhaps as a result of the lower barrier height for the crystal field Γ_7 band caused by the strain and the aluminum content in the barriers. The reordering of these states will cause the ground state to have a Γ_7 character and the inverted spin splitting would account for the observed enhanced effective g factor.

The increase of the value for sample N307 in Fig. 4 with respect to the same width in the other samples can be understood in terms of the distributions of the electric fields. Where more than one quantum well is present, the finite thickness of the barrier allows a redistribution of the polarization fields between both the well and the barrier, whereas the field is solely in the wells for the SQW. This will push the hole states further into the barrier material.

B. Diamagnetic shift

The magnitude of the diamagnetic shift in equation (2) is determined by the size of the exciton wave function in the plane perpendicular to the field. From this it is possible to infer the excitonic binding energy and the following section describes how these parameters have been determined for the different quantum wells along with values corresponding to the bulk case.

The effect of a magnetic field can be considered as an extra confining potential on the already localized excitonic system in both two-dimensional (2D) and 3D cases. The bulk data can be fitted very well to a full numerical calculation for a 3-dimensional hydrogen atom in a magnetic field[16] that uses the excitonic binding energy and the reduced mass as fitting parameters. The binding energy for our particular sample was determined by Neu *et al.*[17] as 24.1 meV by identifying the 2s excited state, and this enables the fitting to give a reduced mass of 0.180(2) m_e as the only free parameter. This numerical calculation reduces to a B^2 dependence in the low-field limit, so that by fitting the low-field data we obtain a coefficient, $\gamma_2=2.04(3)$ μ eV/T^2 that we can use in a direct comparison between the bulk and QW data.

The diamagnetic coefficient for an exciton is given by,[18,19]

$$\gamma_2=\frac{e^2}{8\mu}\langle\rho^2\rangle, \tag{4}$$

where μ is the reduced mass of the exciton and ρ is the separation of the electron and the hole in the plane of the quantum well. Therefore the diamagnetic coefficient contains information about the zero-field properties of the exciton and can give a value for the in-plane extent of the wave function.

From the 1s orbital in the hydrogen atom, the expectation value of r^2 is, $\langle r^2\rangle=3a_0^{*2}$, where a_0^* is the effective Bohr radius. r^2 can then be converted to an in-plane size through $\langle\rho^2\rangle=\frac{2}{3}\langle r^2\rangle$. If the exciton is assumed to remain essentially three dimensional, the effective binding energy R^* can then be deduced through scaling with respect to the hydrogen atom,

$$R^*=\frac{1}{\varepsilon_r}\frac{a_0^H}{a_0^*}R^H, \tag{5}$$

where a_0^H is the Bohr radius and R^H is the Rydberg constant. This gives the following expression:

TABLE III. The in-plane extent and exciton binding energy for the different quantum well widths deduced from the diamagnetic shift of the luminescence.

Sample	Width (Å) (approx.)	In-plane extent of exciton (Å)	Exciton binding energy (meV)
N257			
4 ML	10	28.5 (1.0)	36.5 (1.3)
8 ML	20	33.0 (1.2)	31.5 (1.2)
12 ML	30	41.7 (2.0)	24.9 (1.2)
16 ML	40	49.4 (2.5)	21.0 (1.1)
N298			
4 ML	10	30.0 (1.4)	34.6 (1.6)
8 ML	20	28.3 (1.7)	36.6 (2.2)
12 ML	30	33.9 (1.2)	30.7 (1.1)
N307			
8 ML	20	35.0 (1.2)	39.6 (1.0)
G889			
Bulk	-	40.9 (5)	25.4 (2)

$$R_{3D}^{*}=\sqrt{\frac{e^2}{4\mu}\frac{1}{\gamma_2}}\frac{(a_0^H R^H)_{3D}}{\varepsilon_r}. \tag{6}$$

A similar equation assuming a two-dimensional exciton and hydrogen atom gives a slightly different relationship between these parameters and would predict binding energies larger by a factor $\sqrt{3}$,[20]

$$R_{2D}^{*}=\sqrt{\frac{3e^2}{4\mu}\frac{1}{\gamma_2}}\frac{(a_0^H R^H)_{3D}}{\varepsilon_r}=\sqrt{3}R_{3D}^{*}. \tag{7}$$

The results from this calculation using Eq. (6) assuming a 3D exciton have been summarized in Table III ($\varepsilon_r=9.8$ [Refs. 21 and 22], $\mu=0.18\ m_0$ [Ref. 23]). The similarity of the binding energy for the bulk deduced in this way, 25.3 meV compared to 24.1 meV from the $1s$-$2s$ separation, illustrates the accuracy of this technique. By using the three-dimensional model, these values give the low-energy limits of the quantum well binding energies.

Table III shows that as the well width is reduced, the exciton size is also reduced resulting in a strong enhancement of the binding energy for the narrow wells, in agreement with Bigenwald *et al.*[24] and Grandjean *et al.*[1] We also observe a reduction of the exciton binding energy for the widest well due to the separation of the electron and hole to the separate interfaces of the QW. Our results can be compared with the calculations from Bigenwald *et al.*[24] shown in Fig. 7 and Fig. 8 of the in-plane extent and binding energy of excitons in $GaN/Al_xGa_{1-x}N$ quantum wells for different compositions and well widths.

These variational calculations of the excitonic wave functions were used to investigate the ground state of heavy hole, free excitons under different levels of approximation. Two different forms of the variational ground-state wave function were considered in the calculations. Both included a single variational parameter to govern the lateral extent of the wave function, however for one an additional variational parameter was included in the determination of the separation of the electron and hole along the confinement axis. In the single parameter trial function this separation is solely determined by the electric fields present in the structure, whereas an additional contribution from the Coulomb attraction is allowed for in the two-parameter trial function.

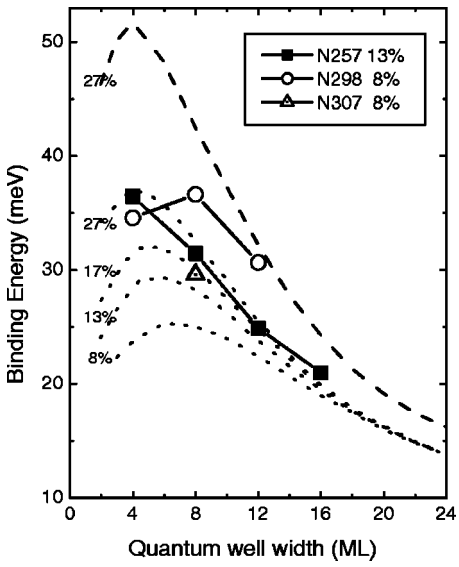

FIG. 8. Experimental values of the binding energies shown with calculations of the well-width dependence of the exciton binding energies for a $GaN/Al_xGa_{1-x}N$ SQW including internal electric fields. For a single parameter variational trial function (short dash), calculations are shown for four aluminum compositions, x= 0.27, 0.17, 0.13, 0.08, whereas for a two-parameter function (long dash), $x=0.27$.

The experimental results from N257 are shown alongside the theoretical calculations of the in-plane pseudo-Bohr radius in Fig. 7. Our results agree well with the theory despite the lower aluminum concentration in the barriers, 13% compared to the value of 27% used in the calculations.

There are larger differences between the binding energies deduced from γ_2, and this can be understood both from the simplicity of our model and the greater influence that the higher aluminum concentration is expected to have through the increased electric field. However the data favors the inclusion of the field rather than its omission in square-well calculations.[24]

The single parameter trial function underestimates the binding energy for a given aluminum composition and the more accurate two-parameter function is shown only for an aluminum composition, $x=0.27$. From comparing results for $x=0.27$ for both models, it seems that the two-parameter function for the appropriate composition, $x=0.08$, and 0.13, would accurately account for the data.

It should be pointed out that the theoretical results are for the heavy-hole exciton, which we have shown is not the lowest state for these samples. This should not be significant for the purposes of comparison because the excitonic mass will be predominantly determined by the electron mass. The

relevant hole mass would be an average over the top of the valence band within an exciton binding energy from the band edge, and is likely to be heavy as a result of the valence band mixing associated with the band reordering. Both theory and experiment use the heavy-hole exciton mass as a first approximation.

In converting from the diamagnetic coefficient γ_2 to the binding energy a three-dimensional model was used as a basis rather than a two-dimensional model. This will have the tendency to underestimate the quantum well binding energy. However the approximation remains reasonable due to both the shrinkage of the in-plane wave function caused by the increased binding and the considerable leakage of the bound-state wave function out of the wells into the barriers. The evidence for this includes both the change in the valence band ordering and the maximum in the theoretical excitonic binding energy at around 4 ML, where the peak value is only 50% of the two-dimensional limit.

The energy shifts that we have discussed are very small in comparison with the linewidth. It is worth thinking of the reasons behind this and the prospects for future experiments. In the field of nitride semiconductors, it has become automatic to blame any sample inadequacies on the lack of a suitably lattice-matched substrate. However recent work on homoepitaxially grown quantum well samples has suggested that there is perhaps a fundamental limitation in the linewidth, similar to the linewidths present in this work, that is caused by the random positions of the group III elements in the ternary barrier combined with the large hole masses.[25,26] The strong internal fields, through causing a strong separation of the electron and hole wave functions to the opposite interfaces of the quantum well, thus make the optical properties very sensitive to these barrier irregularities.

V. CONCLUSIONS

This work has presented magnetoluminescence data in fields up to 55 T for three different GaN/$Al_xGa_{1-x}N$ quantum well samples that shows a strong well-width dependence of the shift of the luminescence peaks. The high-pulsed fields were essential in the resolution of the different dependencies, and even when the immense amount of work on the sample growth in the future is considered with the expected improvement in quality, it is unlikely that this would allow lower continuous fields to be used due to the fundamental linewidth limitations present.

Our data shows that by observing an enhanced g factor for the narrow wells, the valence band must have changed significantly compared with bulk GaN. We have attributed this to a reordering of the valence band states in the strained $Al_xGa_{1-x}N$ barriers, giving different barrier heights for the different quantum well hole states. We have also observed an increase in the exciton binding energy with the reduction of the well width in agreement with calculations using a variational approach in the envelope function formalism that includes the effect of the electric field in the wells. Better agreement is obtained when the trial wave function includes a consideration of the three-dimensional Coulomb potential.

ACKNOWLEDGMENTS

We are grateful to the EPSRC (UK) for the support of this work and particularly the Lasers for Science Facility for the provision of the frequency-doubled argon laser. P.A.S. acknowledges financial support from Sharp Laboratories of Europe Ltd.

[1] N. Grandjean, B. Damilano, S. Dalmasso, M. Leroux, M. Laügt, and J. Massies, J. Appl. Phys. **86**, 3714 (1999).

[2] N. Grandjean, B. Damilano, S. Dalmasso, M. Leroux, M. Laügt, and J. Massies, Phys. Status Solidi A **176**, 219 (1999).

[3] T. Wang, D. Nakagawa, J. Wang, T. Sugahara, and S. Sakai, Appl. Phys. Lett. **73**, 3571 (1998).

[4] The ELOG templates were provided by B. Beaumont and P. Gibart, CRHEA-CNRS, Valbonne, France.

[5] N. Grandjean and J. Massies, Appl. Phys. Lett. **71**, 1816 (1997).

[6] F. Bernardini, V. Fiorentini, and D. Vanderbilt, Phys. Rev. B **56**, R10 024 (1997).

[7] I. V. Kukushkin, N. J. Pulsford, K. von Klitzing, K. Ploog, and V. B. Timofeev, Surf. Sci. **263**, 30 (1992).

[8] P. A. Shields, R. J. Nicholas, B. Beaumont, and P. Gibart, Phys. Status Solidi B **216**, 17 (1999).

[9] R. Stepniewski, M. Potemski, A. Wysmolek, K. Pakula, J. M. Baranowski, J. Luusakowski, I. Grzegory, S. Porowski, G. Martinez, and P. Wyder, Phys. Rev. B **60**, 1 (1999).

[10] W. Knap, E. Frayssinet, M. L. Sadowski, C. Skierbiszewski, D. Maude, V. Falko, M. A. Khan, and M. S. Shur, Appl. Phys. Lett. **75**, 3156 (1999).

[11] G. L. Bir and G. E. Pikus, *Symmetry and Strain-Induced Effects in Semiconductors* (Wiley, New York, 1974).

[12] K. Kim, W. R. L. Lambrecht, and B. Segall, Phys. Rev. B **56**, 7363 (1997).

[13] J. M. Luttinger, Phys. Rev. **102**, 1030 (1956).

[14] Lowest in terms of the hole energy.

[15] 11 and 12 meV from the review in Kim *et al.* (Ref. 12), 14.9 $\pm$0.3 meV from reflectivity of sample G889.

[16] P. C. Makado and N. C. McGill, J. Phys. C **19**, 873 (1986).

[17] G. Neu, M. Teisseire, B. Beaumont, H. Lahreche, and P. Gibart, Phys. Status Solidi B **216**, 79 (1999).

[18] J. J. Hopfield and D. G. Thomas, Phys. Rev. **122**, 35 (1961); R. G. Wheeler and J. O. Dimmock, *ibid.* **125**, 1805 (1962).

[19] S. N. Walck and T. L. Reinecke, Phys. Rev. B **57**, 9088 (1998).

[20] M. Shinada and S. Sugano, J. Phys. Soc. Jpn. **21**, 1936 (1966).

[21] 3D average; $\varepsilon=(\varepsilon_\perp)^{2/3}(\varepsilon_\parallel)^{1/3}$.

[22] A. S. Barker, Jr. and M. Ilegems, Phys. Rev. B **7**, 743 (1973).

[23] This value is taken from the bulk calculations and is used as a first approximation. The actual value will depend on the precise band ordering and mixing effects as described in the section entitled Zeeman splitting.

[24] P. Bigenwald, P. Lefebvre, T. Bretagnon, and B. Gil, Phys. Status Solidi B **216**, 371 (1999).
[25] N. Grandjean, B. Damilano, J. Massies, G. Neu, M. Tessiere, I. Grzegory, S. Porowski, M. Gallart, P. Lefebvre, B. Gil, and M. Albrecht, J. Appl. Phys. **88**, 183 (2000).
[26] M. Gallart, A. Morel, T. Taliercio, P. Lefebvre, B. Gil, J. Allegre, H. Mattieu, N. Grandjean, M. Leroux, and J. Massies, Phys. Status Solidi A **180**, 127 (2000).